Original Paper

Geochemistry and genesis of marine shallow gas in the Pearl River Mouth Basin (PRMB), South China Sea

Wei Si [a,b,c], Du-Jie Hou [a,b,c,*], Xiong Cheng [a,b,c]

[a] School of Energy Resources, China University of Geosciences (Beijing), Beijing, 100083, China
[b] Key Laboratory of Marine Reservoir Evolution and Hydrocarbon Enrichment Mechanism, Ministry of Education, Beijing, 100083, China
[c] Beijing Key Laboratory of Unconventional Natural Gas Geological Evaluation and Development Engineering, Beijing, 100083, China

A R T I C L E I N F O

Article history:
Received 11 November 2024
Received in revised form
11 April 2025
Accepted 1 August 2025
Available online 6 August 2025

Edited by Xi Zhang and Jie Hao

Keywords:
Shallow gas
Geochemistry
Gas escape
Microbial activity
Carbon dioxide reduction
Baiyun Sag

A B S T R A C T

In the Pearl River Mouth Basin of the northern South China Sea, extensive commercial shallow gas reservoirs have recently been discovered. However, their formation mechanisms remain poorly constrained. This study employs integrated petroleum geological and geochemical shalix[1ɣN]CTUp7EKZET x'

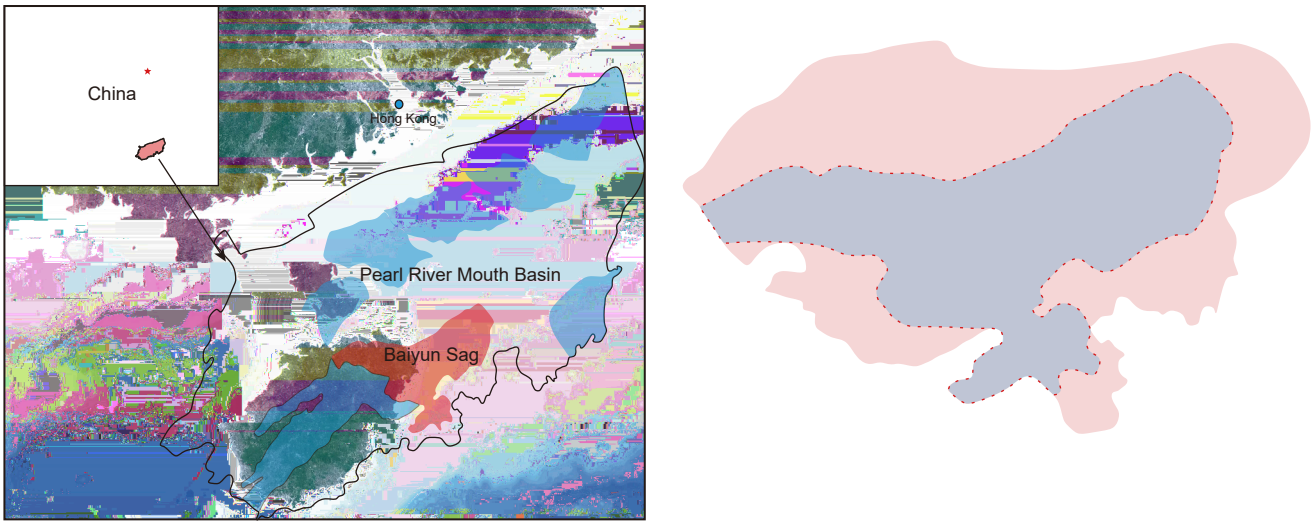

Fig. 1. (**a**) Geographic setting of the Pearl River Mouth Basin and Baiyun Sag. (**b**) Distribution of the sampling wells.

complicates gas-source correlation (Jiang et al., 2015; Ping et al., 2021; Xu et al., 2021), particularly when conventional isotopic proxies are confounded by secondary alterations. The distinct geochemical signatures and accumulation mechanisms of shallow gas, contrasting with deep reservoirs, are poorly constrained, hindering the development of unified exploration models. This study leverages comprehensive geochemical data, including molecular and isotopic analyses of 44 shallow gas samples, to address these knowledge gaps. By integrating light hydrocarbon analysis, carbon isotope fractionation patterns, and biomarker data, we aim to: (1) elucidate the genetic mechanisms of shallow gas, distinguishing between biogenic, thermogenic, and mixed-source contributions; (2) quantify the relative proportions of microbial and thermogenic gases using end-member mixing models; (3) develop a conceptual model for shallow gas accumulation, highlighting the roles of migration pathways, microbial activity, and preservation conditions. By addressing these scientific and practical challenges, this work contributes to the growing body of knowledge on shallow gas systems, offering new insights into their genesis and accumulation mechanisms in the PRMB and beyond.

2. Geological setting

The Pearl River Mouth Basin, located on the northern South China Sea's continental shelf, stretches northeast-southwest over about 2.5×10^5 km^2 (Fig. 1(a)). Ranked as one of China's largest offshore petroleum basins by area, it has produced over 3×10^8 t of oil and 3.5×10^{10} m^3 of natural gas (Zhang et al., 2021). This Mesozoic–Cenozoic passive margin rift basin exhibits a zonal distribution: oil-dominated reservoirs cluster in the Zhu I Depression and Dongsha Uplift, while gas fields prevail in the Baiyun Sag and Panyu Low Uplift (Fig. 1(b)). The basin's tectonic evolution comprises three principal phases (Jiang et al., 2015; Ping et al., 2021): (1) Late Cretaceous–Oligocene Rifting Phase, characterized by NE-trending normal faults controlling half-graben development, accompanied by lacustrine and deltaic sedimentation; (2) Miocene Post-Rift Subsidence, dominated by thermal subsidence and widespread delta-to-shelf deposition, with reactivation of deep-seated faults facilitating fluid migration (Xu et al., 2021); and (3) Pliocene–Quaternary Rapid Subsidence, driven by South China Sea spreading, forming deep-water slope systems and gas hydrate stability zones. Primary gas reservoirs are hosted in the Oligocene–Miocene strata (Fig. 2).

The Baiyun Sag, the deepest depocenter (>12 km Cenozoic sediments), is bounded by the oceanic crust to the south and the Panyu Uplift to the north (Jiang et al., 2015; Ping et al., 2021; Xu et al., 2021). Deep-seated NWW-trending faults, penetrating the Moho, act as conduits for mantle-derived CO_2 and thermogenic hydrocarbons (Yang et al., 2022). Gas chimneys and mud diapirs, identified through three-dimensional seismic imaging, delineate focused fluid migration pathways (Sun et al., 2012). The Baiyun Sag is the basin's subsidence center, with water depths from approximately 200 m to 2800 m. Sediments derived predominantly from the Paleo-Pearl River exhibit unidirectional transport patterns (Fig. 1). Stratigraphically, the succession comprises: Eocene Wenchang Formation (lacustrine deposits), Enping Formation (shallow lacustrine-delta plain systems), Oligocene Zhuhai Formation (deltaic-continental shelf sequences), Miocene Zhujiang, Hanjiang, and Yuehai Formations (deltaic-slope deposits), Pliocene–Quaternary siliciclastic sediments (Fig. 2) (Ping et al., 2021; Xu et al., 2021). Thermogenic source rocks are developed in the Wenchang, Enping, and Zhuhai formations (Jiang et al., 2015; Ping et al., 2021; Xu et al., 2021), while biogenic gas-prone rocks are restricted to the Hanjiang Formation and its suprajacent successions (Fig. 2).

3. Samples and methods

This study examined 44 drilling stem test (DST) gas samples from 12 exploratory and production wells in shallow commercial gas reservoirs (Fig. 1(a)). Sampling locations included the Yuehai-Hanjiang Formation of the Panyu uplift, the Hanjiang Formation at the Baiyun Sag center, and the Zhujiang-Zhuhai Formation in the southern sag's deep-water zone (Figs. 1(b) and 2). Hydrocarbon composition was determined using a modified Agilent Technologies 7890B gas chromatograph (GC) with a triple-channel system. Channel A, suitable for analyzing hydrocarbon gases, uses helium as the carrier gas with a flame ionization detector (FID). GC conditions for Channel A include a Varian 2378 column (KC5 50 m × 0.53 mm) with helium as the carrier gas; the initial temperature is held constant for 3 min, then ramped at 25 °C/min to 190 °C, followed by another 3-min hold. Channel B, designed for the analysis of carbon dioxide (CO_2), hydrogen sulfide (H_2S),

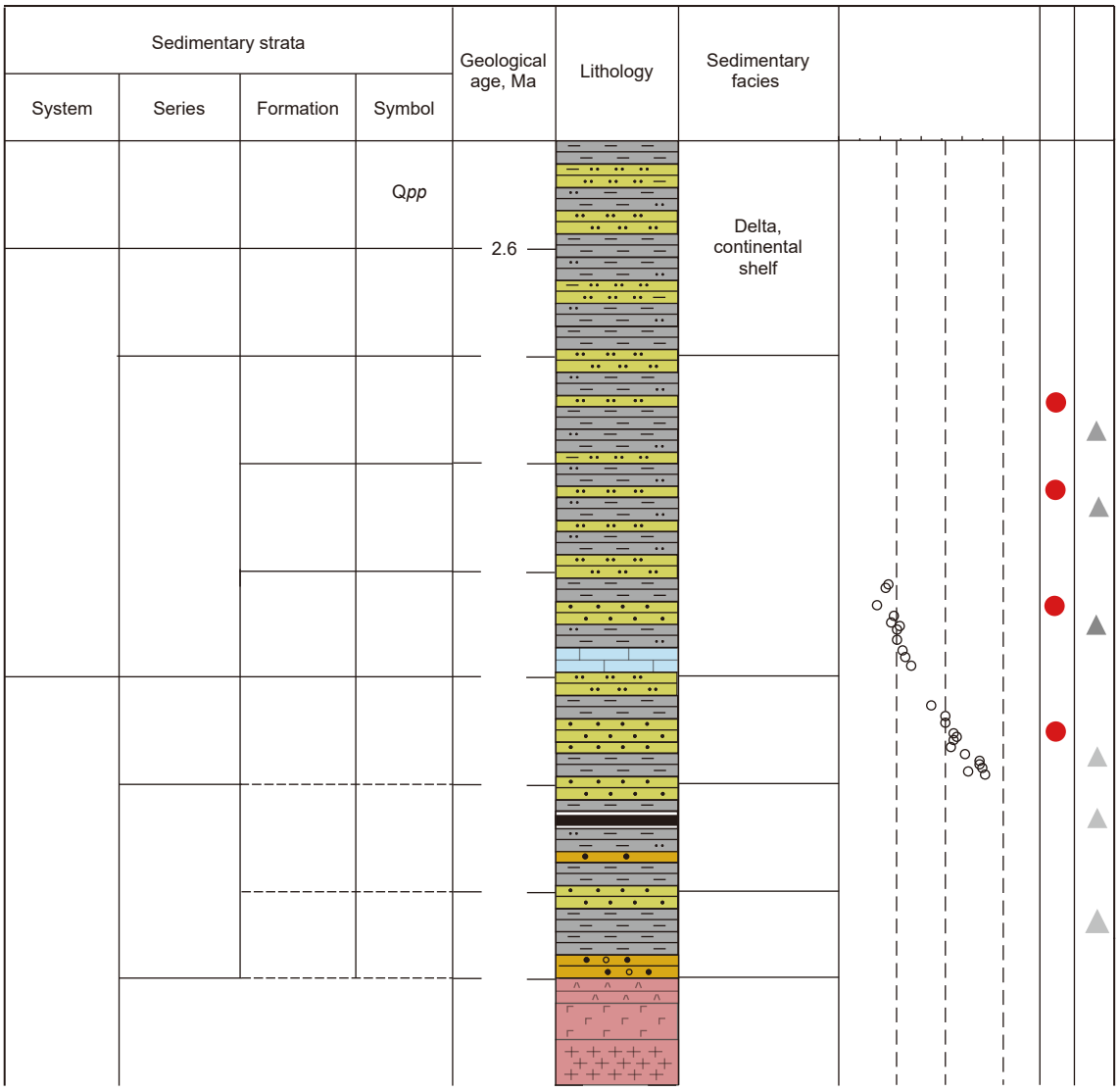

Fig. 2. Generalized stratigraphic column of the Baiyun Sag and Panyu Uplift in the Pearl River Mouth Basin, modified from Ping et al. (2021) and Xu et al. (2021), depicting geological age, sedimentary facies, organic matter maturity, gas enrichment intervals, and source rock layers. Vitrinite reflectance (%) data are from well B52 in the central region of the Baiyun Sag. The hydrocarbon generation model follows Tissot et al. (1974).

oxygen (O_2), nitrogen (N_2), carbon monoxide (CO), and methane (CH_4), employs a helium carrier gas with a stainless-steel molecular sieve packed column at a constant temperature of 90 °C, utilizing thermal conductivity detector (TCD). Channel C, intended for hydrogen (H_2) analysis, uses nitrogen as the carrier gas with a stainless-steel molecular sieve-packed column, operating at a constant temperature with TCD detection. Quantification employed the external standard method, with component relative concentrations normalized post-analysis. Individual compounds were separated using an Agilent 7890B GC, while carbon isotopes were measured with a GV Instruments Isoprime mass spectrometer connected to an Agilent Technologies 6890N GC (GC-IRMS), adhering to the Vienna PeeDee Belemnite (VPDB) standard. Hydrogen isotopes were determined using a Delta VADVANTAGE mass spectrometer with a VARIAN-PLOT FUSED chromatographic column, referenced to the Vienna Standard Mean Ocean Water (VSMOW) standard. All samples underwent ≥4 (carbon isotopes) or ≥3 (hydrogen isotopes) replicate analyses, with means reported as final values.

Mudstone and oil sand samples were extracted from fresh core samples of the Yuehai and upper Hanjiang formations. These core samples were crushed to 120 and 80 meshes, respectively, and extracted with dichloromethane for 72 h using the Soxhlet extraction method, followed by group composition separation (saturated hydrocarbons, aromatic hydrocarbons, non-hydrocarbons, asphaltenes). Saturated hydrocarbon fractions (~20 mg) were analyzed via Agilent 7890A-5973C GC-MS following the Chinese standard GB/T 18606–2017. All laboratory procedures

were conducted in the Key Laboratory of Marine Reservoir Evolution and Hydrocarbon Enrichment Mechanism, Ministry of Education. Chromatographic data of crude oil and formation temperature profiles were provided by CNOOC (Shenzhen) Co., Ltd. Hydrogen and oxygen isotopic compositions of formation water in the Pearl River Mouth Basin were sourced from Xiao et al. (2015).

4. Geochemical characterization and mixed-source quantification of shallow gas reservoirs

4.1. Geochemical characterization of shallow gas

The shallow gas exhibits a distinct vertical layering pattern (Fig. 3(a)). Methane in shallow reservoirs has relatively lighter carbon isotopic compositions (δ^{13}C-CH_4: −70‰ to −35‰) compared to deeper thermogenic gas (δ^{13}C-CH_4 > −40‰). The gas dryness coefficient ($C_1/[C_1–C_5]$) initially decreases and then increases with depth, with an inflection point at approximately 2000 m, corresponding to a minimum *in situ* formation temperature of ~80 °C (Fig. 3(c)). This depth-temperature threshold marks the current upper limit for microbial methane production in the Baiyun Sag, except for some thermophilic methanogens (Fig. 3(c)) (Wilhelms et al., 2001). Below this depth, thermogenic processes dominate, with increasing gas maturity and heavier $C_1/(C_1–C_5)$ values (Fig. 3(b)). Conversely, at shallow depths, lower temperatures favor microbial activity, producing biogenic gas characterized by lighter δ^{13}C-CH_4 values (<−55‰) and elevated $C_1/(C_1–C_5)$ ratios (>0.99). Thermogenic gas contributions to shallow reservoirs exhibit spatial heterogeneity, constrained by the development of vertical migration pathways (Sun et al., 2012). Reservoirs devoid of such conduits demonstrate biogenic gas predominance at shallow depths, characterized by increased elevated methane dryness indices and δ^{13}C-CH_4 depletion (Fig. 3(a) and (b)). The lower depth limit for shallow gas remains debated, with proposed ranges of 1000–2000 m (Gao et al., 2010; Mueller et al., 2018). For the Baiyun Sag, a 2000 m threshold is adopted based on the observed burial depth distribution (300–1600 m) and compositional trends, including biogenic gas dominance above 2000 m (Fig. 3) and regional thermal constraints on current microbial activity (≤80 °C; Fig. 3) (Wilhelms et al., 2001).

Shallow gas reservoirs exhibit $C_1/(C_1–C_5)$ ratios >0.9 and δ^{13}C-CH_4 values ranging from −52‰ to −34.4‰ (Fig. 4(b)). A threshold $C_1/(C_1–C_5)$ ratio of 0.95 demarcates distinct genetic regimes: below this threshold, δ^{13}C-CH_4 increases proportionally with $C_1/(C_1–C_5)$, whereas ratios >0.95 indicate mixed-origin gases characterized by inverse δ^{13}C-CH_4 enrichment (Fig. 4(a)). Except for the W211 well, dominated by biogenic methane ($C_1/[C_1–C_5]$ > 0.97, δ^{13}C-CH_4 = −50‰), shallow reservoirs contain heavier carbon isotopes of ethane and propane compared to deeper gas (Fig. 4(b) and (c)). Carbon isotopic compositions typically follow a normal distribution pattern, increasing from CH_4 to C_4H_{10} (Fig. 5). Only gas from well W211 shows unique carbon isotope distributions (Type II, III, and IV), whereas carbon isotopes from other reservoirs are similar (Type I), indicating different sources of organic matter.

Heavier carbon isotopes in natural gas generally result from: (1) rapid escape of lighter isotopes (mass fractionation effect) (Xia and Tang, 2012; Liu et al., 2019); (2) biodegradation, where bacteria consume ^{12}C, enriching ^{13}C in the remaining gas, characterized by high ratios of i-C_4/n-C_4 and i-C_5/n-C_5, as well as the inversion of carbon isotope values (δ^{13}C-CH_4 < δ^{13}C-C_2H_6 < δ^{13}C-C_3H_8 > δ^{13}C-C_4H_{10}) (Larter and di Primio, 2005; Shuai et al., 2011; Liu et al., 2019); (3) ^{13}C enrichment due to water solubility differences (dissolution fractionation effect) (Zhang et al., 1995); (4) source facies or thermal maturity variations, with humic-type gas having heavier isotopes than sapropelic-type; (5) thermochemical sulfate reduction (TSR) (Liu et al., 2019); (6) bacterial sulfate reduction (BSR) (Lin et al., 2016). While deep-seated faults can transport mature thermogenic gas to shallow reservoirs (e.g., Baiyun Sag gas chimneys), three factors preclude shallow gas maturity exceeding source levels. (1) Preferential loss of ^{12}C-enriched methane increases δ^{13}C of residual gas but does not elevate thermal maturity indices (C_2/C_3 ratios, δ^{13}C-C_2) (Xia and Tang, 2012). (2) Biogenic methane dilutes migrated thermogenic gas maturity signals. (3) Shallow temperatures (<80 °C) inhibit oil-to-gas cracking that could theoretically increase maturity (Hunt, 1996). Basin-wide vitrinite reflectance (VR) profiles demonstrate decreasing VR values with shallower burial depths (Fig. 2). Gas maturity parameters (C_2/C_3, δ^{13}C-C_2H_6) in shallow reservoirs consistently align with adjacent mid-mature source rocks (Enping Formation, VR = 0.6%–0.8%), not deeper overmature intervals (Wenchang

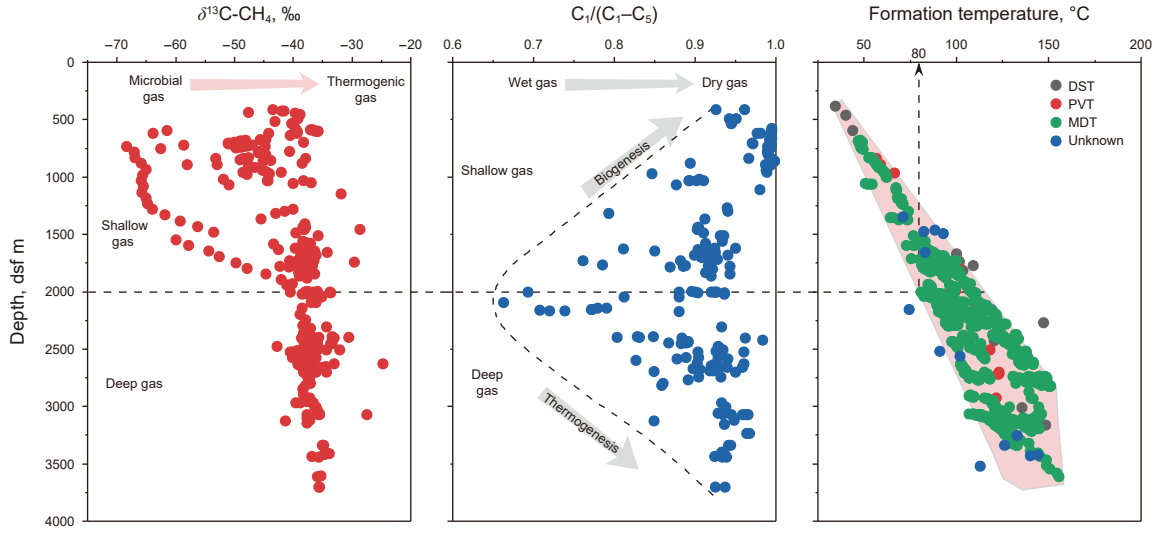

Fig. 3. Cross-plots of (**a**) natural gas methane carbon isotope values (δ^{13}C-CH_4), (**b**) dryness coefficients ($C_1/[C_1–C_5]$), and (**c**) formation temperature with actual depth, displaying the differences in geochemical properties between shallow and deep gas layers. To establish robust geochemical trends, we supplemented the DST data with drilling mud gas (mud logging), PVT samples, headspace gas from core and cuttings, and wellhead gas for production-stage characterization. Abbreviations: bsf, below seafloor; DST, drilling stem test; MDT, modular dynamic test; PVT, pressure-volume-temperature test.

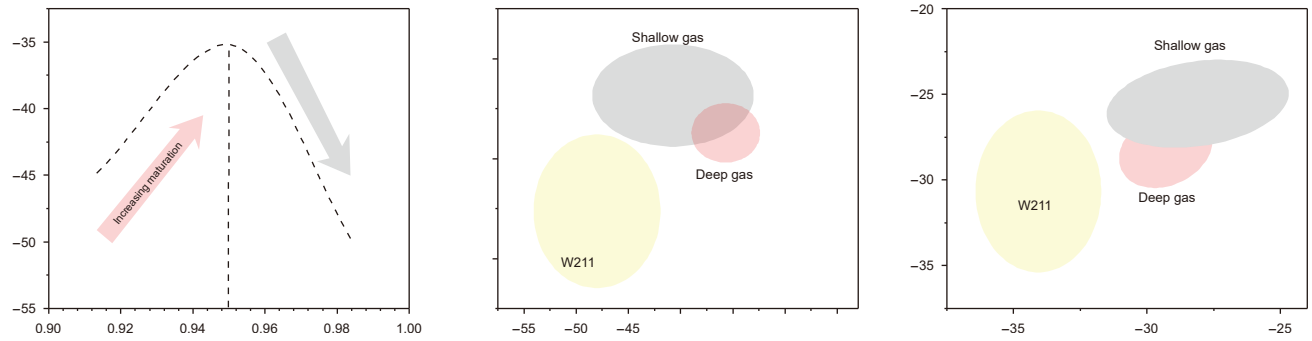

Fig. 4. Geochemical characteristics of gases in shallow gas reservoirs. (**a**) $C_1/(C_1–C_5)$ vs. $\delta^{13}C$-CH_4; (**b**) $\delta^{13}C$-CH_4 vs. δ^{13}-C_2H_6; (**c**) δ^{13}-C_2H_6 vs. $\delta^{13}C_3$-C_3H_8.

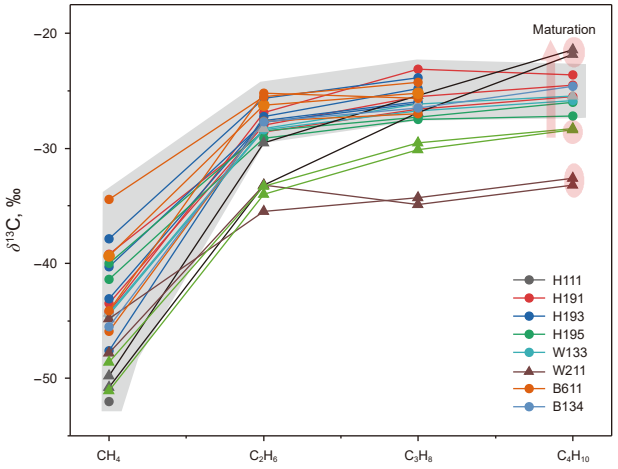

Fig. 5. Distribution characteristics of $\delta^{13}C$-CH_4 to $\delta^{13}C$-C_4H_{10} in shallow gas reservoirs.

Formation, VR > 1.2%) (Ping et al., 2021). Secondary alteration enriching ^{13}C is typically mediated by aerobic bacteria. However, biological methane production activities are frequently observed in the shallow layers, indicating strictly anaerobic environments (Schoell, 1980; Whiticar, 1999). Low *i*-C_4/*n*-C_4 and *i*-C_5/*n*-C_5 ratios (<2; H195, Table 1) and rare $\delta^{13}C$ inversions ($\delta^{13}C$-CH_4 < $\delta^{13}C$-C_2H_6 < $\delta^{13}C$-C_3H_8 > $\delta^{13}C$-C_4H_{10}) further negate biodegradation. Negligible H_2S concentrations (H195, Table 1) and reservoir depths (>300 mbsf) below sulfate-methane transition zones (SMTZs; <10 mbsf regionally) eliminate TSR/BSR as viable ^{13}C-enrichment pathways (Lin et al., 2016).

For natural gas in free-phase migration, the N_2 concentration ($\delta^{13}C$-C_2H_6–$\delta^{13}C$-CH_4) and saturate/aromatic values are reliable indicators of migration direction (Prinzhofer et al., 2000; Ye et al., 2017). These proxies prove unreliable in shallow gas due to biogenic gas influence, causing ($\delta^{13}C$-C_2H_6–$\delta^{13}C$-CH_4) values and N_2 concentrations to be higher in shallow layers than in deeper intervals. The H195 gas samples demonstrate depth-dependent aromatic hydrocarbon depletion, exemplified by decreasing benzene/normal hexane and toluene/normal heptane ratios upward (Table 1). Enhanced adsorption of polar aromatic compounds onto reservoir matrices, compared to saturated hydrocarbons, drives this compositional fractionation (Huang et al., 2022). Shallow layers in the Baiyun Sag, particularly the Yuehai and Hanjiang formations, feature marine saline water deposits, contrasting with thermogenic gas source rocks in lacustrine and shallow marine deltaic environments. The elevated salinity in shallower strata, coupled with declining formation pressure at reduced burial depths, restricts aqueous-phase gas migration to overlying layers. Natural gas molecules' small size and high mobility allow strong breakthrough capabilities. Poor diagenetic consolidation in shallow caprocks further reduces seal integrity (Li et al., 2008), establishing a dynamic equilibrium between gas charging and diffusive losses (Dang et al., 2008). Mass-dependent isotopic fractionation favors ^{12}C diffusion over ^{13}C due to its lower mass, leading to partial gas dissipation and forming hydrates at the shallow seabed (Dai et al., 2017). While methane loss theoretically enriches $\delta^{13}C$, microbial input dominates the isotopic signal (Fig. 3), masking this effect. Ethane/propane experiences slower diffusion but stronger ^{13}C enrichment due to molecular mass constraints (Liu et al., 2019). Residual C_{2+} thus shows heavier $\delta^{13}C$. In conclusion, heavy carbon isotopes present in shallow gas are primarily attributed to preservation conditions.

In the study area, shallow gas reservoirs mainly consist of hydrocarbon gases. Non-hydrocarbon gases, primarily N_2 and CO_2, are present in relatively low concentrations, typically <5% and <1%, respectively (Fig. 6 and Table 1). CO_2 exhibits $\delta^{13}C$ values spanning from −28.6‰ to −4.4‰ (Fig. 6), suggesting inorganic contributions ($\delta^{13}C$-CO_2 > −8‰ or CO_2 > 60%) (Dai et al., 1996), potentially from mantle or microbial sources. In the gas layers of the Well W211 (Fig. 6), CO_2 constitutes 60% of the volumetric composition, with $\delta^{13}C$ values surpassing −5‰ and R/R_a (i.e., the ratio of measured $^3He/^4He$ to atmospheric $^3He/^4He$) > 6.5 (Yang et al., 2022), characteristic of mantle-derived inputs. Mud

Table 1
Molecular composition (%) of gas reservoirs (ZJ450, Z310, HJ610, HJ410) in Well H195.

Well	Reservoirs	Gas composition, vol%											Ben/*n*-C_6	Tol/*n*-C_7	*i*-C_4/*n*-C_4	*i*-C_5/*n*-C_5
		C_1	C_2	C_3	*i*-C_4	*n*-C_4	*i*-C_5	*n*-C_5	C_{6+}	H_2S	N_2	CO_2				
H195	HJ410	92.57	3.67	1.39	0.32	0.34	0.16	0.08	0.27	nd.	0.63	0.57	0.11	0.55	0.94	2.00
H195	HJ610	91.28	4.21	1.49	0.31	0.34	0.15	0.08	0.22	nd.	0.89	1.03	0.18	0.67	0.91	1.88
H195	ZJ310	87.80	3.89	1.37	0.26	0.31	0.13	0.07	0.21	nd.	1.65	4.31	0.56	1.00	0.84	1.86
H195	ZJ450	88.12	4.05	1.52	0.30	0.34	0.14	0.09	0.53	nd.	0.56	4.35	0.60	1.06	0.88	1.56

Abbreviations: Ben/*n*-C_6, benzene/normal hexane; Tol/*n*-C_7, toluene/normal heptane; vol, volume; nd., not determined.

diapirs, gas chimneys, and deep-seated faults in the Baiyun Sag provide migration pathways for deep fluids (Fig. 13). Geochemical data confirm that mantle-sourced CO_2 dominates Pearl River Mouth Basin reservoirs (Huang et al., 2015; Yang et al., 2022).

4.2. Determination of microbial gas proportion

Variations in gas enrichment patterns are influenced by underlying genesis mechanisms, necessitating the quantification of source-specific gas contributions. In the Shenhu Sea area, natural gas hydrates primarily form through the dissipation of biogenic gas into the shallow seabed (Dai et al., 2017). Consequently, the biogenic gas supply critically controls hydrate resource potential. This study employed an end-member gas mixing model (Eq. (1)) to determine microbial gas proportions. The carbon isotopic composition of the mixed gas is jointly controlled by the carbon isotopes and component concentrations of the end-member gases:

$$\delta^{13}C_n = \left(\delta^{13}C_n\,[A] \times V_n\,[A] \times X + \delta^{13}C_n\,[A] \times V_n\,[B][1-X]\right) \Big/ \left(V_n[A] \times X + V_n[B] \times [1-X]\right) \quad (1)$$

where $\delta^{13}C_n$ is the isotopic value of C_n in the mixed gas, ‰; n = carbon number (1 for methane, 2 for ethane, etc.); $Vn[A]$ and $Vn[B]$ denote the relative contents of C_n in end-member A and B; X signifies the volume fraction of end-member A, and [1-X] represents c.);

facies, with kerogen carbon isotope ratios exceeding −25‰ (Ping et al., 2021), distinguishing it from conventional marine-terrestrial systems. As discussed in Section 4.1, shallow gas has elevated carbon isotope values of ethane and propane due to gas escape (Fig. 3). Biogenic gas admixture further obscures genetic interpretations of source rock signatures via conventional carbon isotope analysis.

Biogenic gas's negligible C_{2+} content renders light hydrocarbons (C_{5+}) diagnostic of thermogenic processes, including origin, maturity, and alteration. Light hydrocarbon generation pathways and kinetics vary with the thermal regime, pressure, and kerogen type (Thompson, 1979, 1983; Dai, 1993; Ten Haven, 1996; Huang et al., 2022). Normal heptane (n-C_7) is primarily from bacteria and algae (Thompson, 1979, 1983; Dai, 1993), serving as a dependable maturity indicator due to its progressive enrichment during catagenesis. Methylcyclohexane (MCH) primarily derives from the cellulose, lignin, and carbohydrates found in higher plants (Clayton et al., 1991; Huang et al., 2022), exhibiting relatively stable thermodynamic properties (Huang et al., 2022). Dimethylcyclopentane (DMCP) mainly comes from the cyclic lipid bodies of aquatic organisms (Dai, 1993). The paraffin index, which includes the heptane and isoheptane values, effectively discriminates kerogen type and maturity (Thompson, 1983).

Natural gas in the Enping Formation of Well W132 (southern sag) exhibits biased sapropelic kerogen affinity (Figs. 9 and 10(a)). Thermogenic gas from Well W211 displays depleted δ^{13}C-C_2H_6, δ^{13}C-C_3H_8, and δ^{13}C-C_4

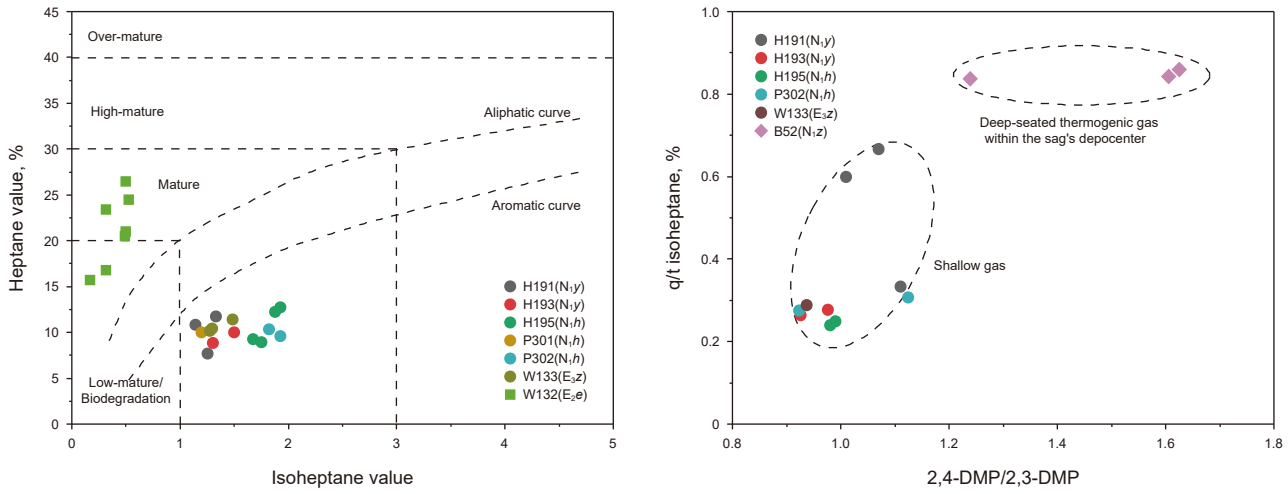

Fig. 10. Heptane light hydrocarbon indices to characterize thermal maturity and source facies of shallow thermogenic gas. (**a**) Isoheptane value vs. Heptane value, modified from Cheng et al. (1987). (**b**) 2,4-DMP/2,3-DMP vs. q/t isoheptanes. The maturity proxies in Fig. 10(b) are quoted from Chung et al. (1998). Heptane value = 100 × (heptane/[the compounds detected between cyclohexane and methylcyclohexane on the chromatogram, but with the omission of l,cis-2-dimethylcyclopentane]); Isoheptane value = (2-methyhexane + 3-methyhexane)/(1,c-3-dimethycyclopentane + 1,t-3-dimethycyclopentane + 1,t-2-dimethycyclopentane); 2,4-DMP/2,3-DMP, 2,4-dimethylcyclopentane/2,3-dimethylcyclopentane; q/t isoheptanes = (2,2-dimethypentane + 3,3-dimethypentane)/(3-ethylpentane + 2,3-dimethypentane + 2,4-dimethypentane).

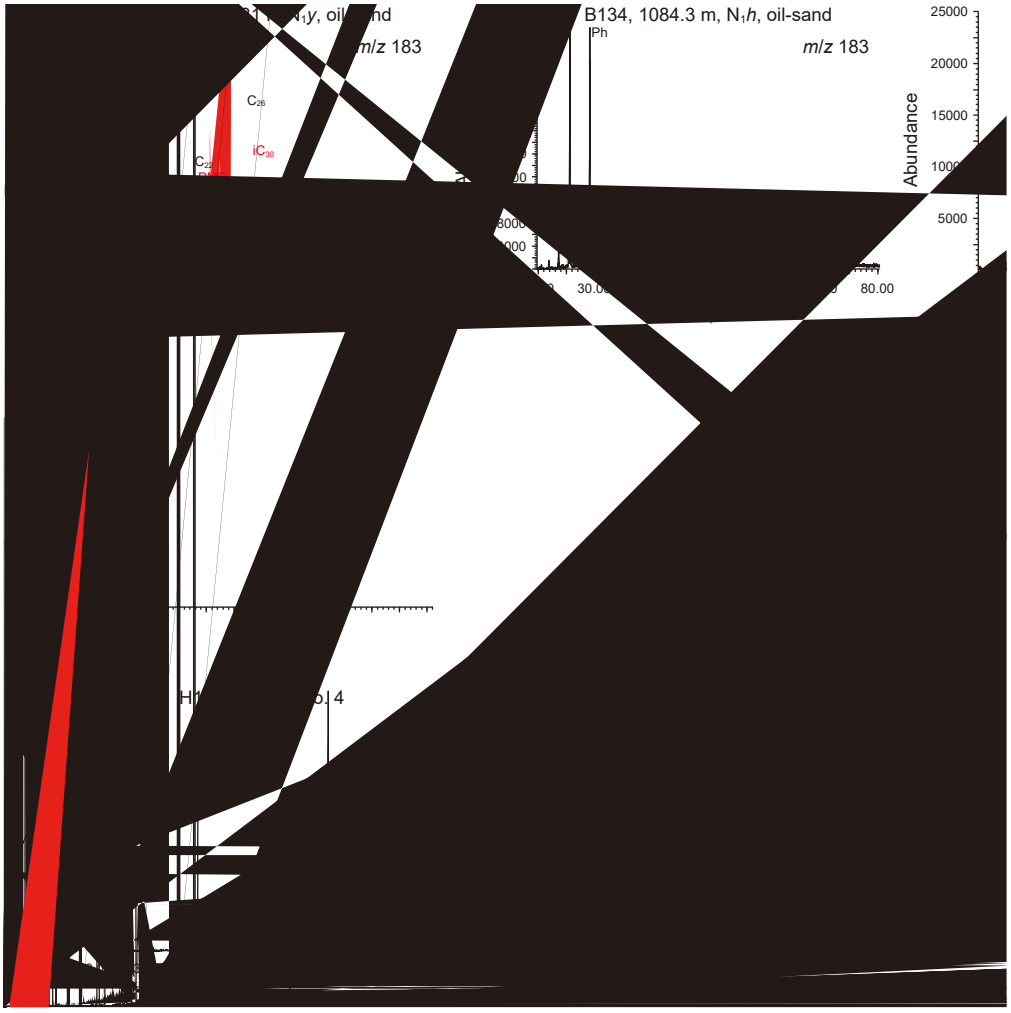

Fig. 11. Total ion flow and selected ion mass spectra of saturated hydrocarbons from mudstone, oil-sand, and crude oil extracts in the study area. The biodegradation process is depicted in Fig. 11(d)–(g), showing a gradual decrease in the relative content of normal and isoprenoid alkanes until they nearly disappear, with a concurrent increase in C_{30} hopanes/(pristane + phytane) values. However, C_{25} norhopanes were not detected (Fig. 11(h) and (i)).

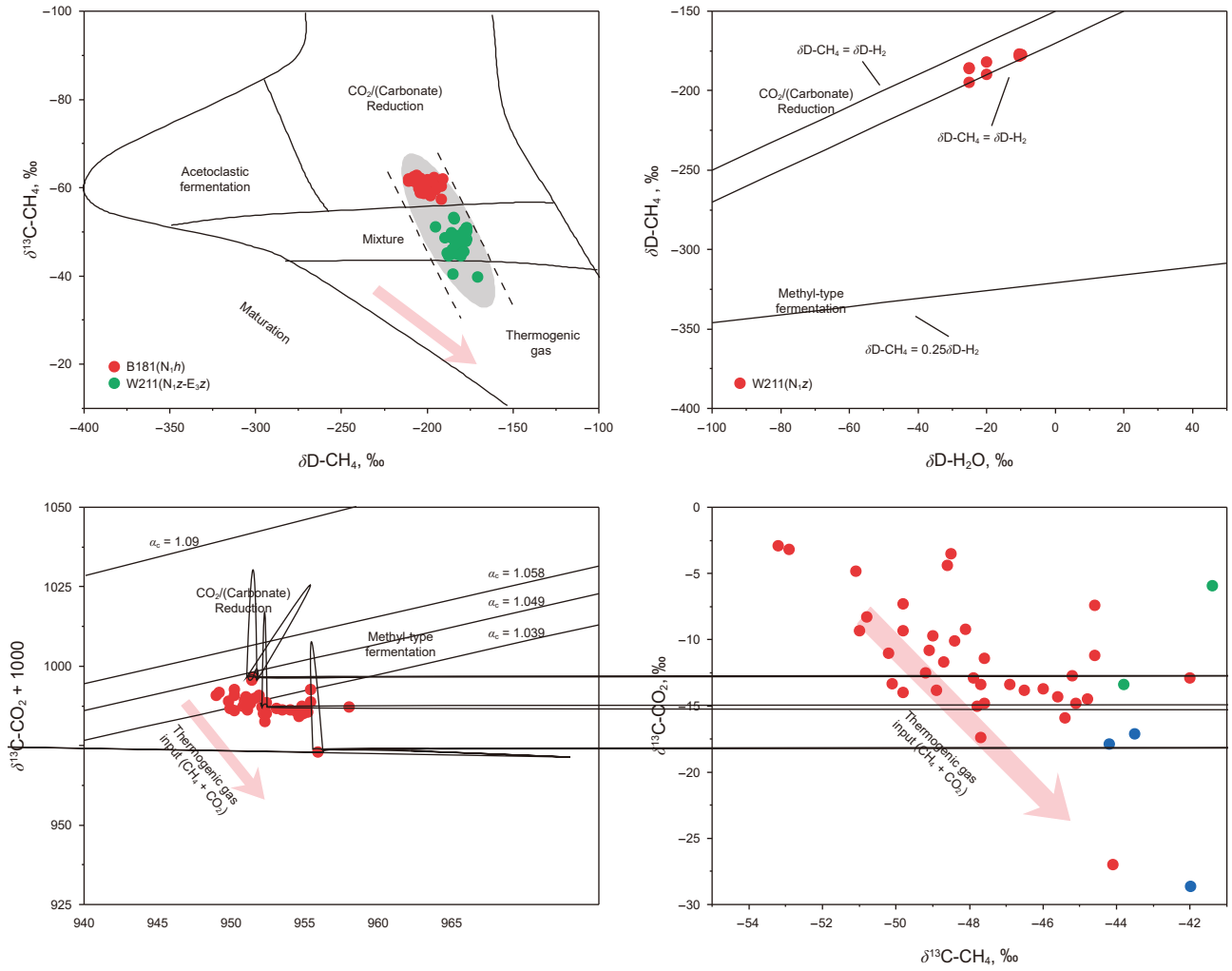

Fig. 12. Determination of biogenic gas generation pathways. (**a**) δD-CH_4 vs. δ^{13}C-CH_4, modified from Whiticar (1999); (**b**) δD-H_2O vs. δD-CH_4, modified from Schoell (1980) and Whiticar (1999); (**c**) (δ^{13}C-CH_4 + 1000) vs. (δ^{13}C-CO_2 + 1000), modified from Whiticar (1999); (**d**) δ^{13}C-CH_4 vs. δ^{13}C-CO_2.

methanogen activity (Fig. 11(a)–(c)), specifically 2, 6, 10, 15, 19-pentamethyleicosane (PMI) and 2, 6, 10, 15, 19, 23-hexamethyltetracosane (squalane) (Brassell et al., 1981), with relative abundances reflecting microbial intensity. Methanogenesis occurs via five metabolic pathways: hydrogenotrophic (utilizing CO_2 and HCOOH), acetoclastic (involving CH_3COOH), methylotrophic (involving substrates like CH_3OH, CH_3NH_2), methoxyl (lignocellulose-derived), and alkylotrophic (using hydrocarbons) (Schoell, 1980; Whiticar, 1999; Lloyd et al., 2021; Zhou et al., 2022). Global primary biogenic reserves predominantly form through CO_2 reduction or a combination of CO_2 reduction and acetate fermentation (Flores et al., 2008; Wang et al., 2022). In the study area, typical oil-biodegradation gas (δ^{13}C-CH_4 < −50‰, C_1/[C_1–C_5] > 0.99, high N_2 concentrations) was identified in the H111 block. Crude oil samples exhibit biodegradation characteristics (Fig. 11(d)–(g)), albeit to a limited extent, as evidenced by the absence of significant 25-norhopane (Fig. 11(h) and (i)). Limited heavy oil reservoir development further restricts oil-degradation gas contributions.

Biogenic gas is governed by methanogenic pathways (Schoell, 1980; Whiticar, 1999). The kinetic isotope effect (KIE) of methane exhibits pathway-specific variability, typically decreasing in the sequence: methylotrophic > hydrogenotrophic > acetoclastic (Krzycki et al., 1987; Whiticar, 1999). Mechanistic divergence between pathways dictates isotopic signatures: acetoclastic methanogenesis derives 25% of methane hydrogen from water and 75% from acetate methyl groups, whereas CO_2 reduction exclusively sources hydrogen from water. This results in distinct δ^{13}C-CH_4 and δD-CH_4 values (Whiticar et al., 1986; Whiticar, 1999). Methane hydrogen isotopes further correlate with coexisting water δD-H_2O (Whiticar, 1999):

$$\delta\text{D - CH}_4\ (‰) = f\ (\delta\text{D - H}_2\text{O} - 160) + (1 - f) \times (0.75 \times \delta\text{D - CH}_4 + 0.25 \times \delta\text{D - H}_2\text{O}) \quad (2)$$

where f denotes the proportion of gas from CO_2 reduction, ranging from 0 to 1. CO_2 reduction exhibits 160‰ (±10‰) between δD-CH_4 and δD-H_2O. Marine and saline lake settings dominated by CO_2 reduction yield δD-CH_4 values exceeding −190‰ (Schoell, 1980), while continental analogs show δD-CH_4 values ranging from −270‰ to −190‰ (Ni et al., 2013). Freshwater environments, with elevated H_2 availability, favor depleted δD-CH_4 values (Whiticar et al., 1986). This feature is reflected in the methane produced by acetate fermentation, which has a heavier carbon isotope ratio and a lighter hydrogen isotope ratio. In the study area, shallow marine-deltaic to shelf facies host brackish-saline environments (Fig. 2). Gas samples from the Hanjiang Formation indicate pure biogenic gas, with δ^{13}C-CH_4 values ranging

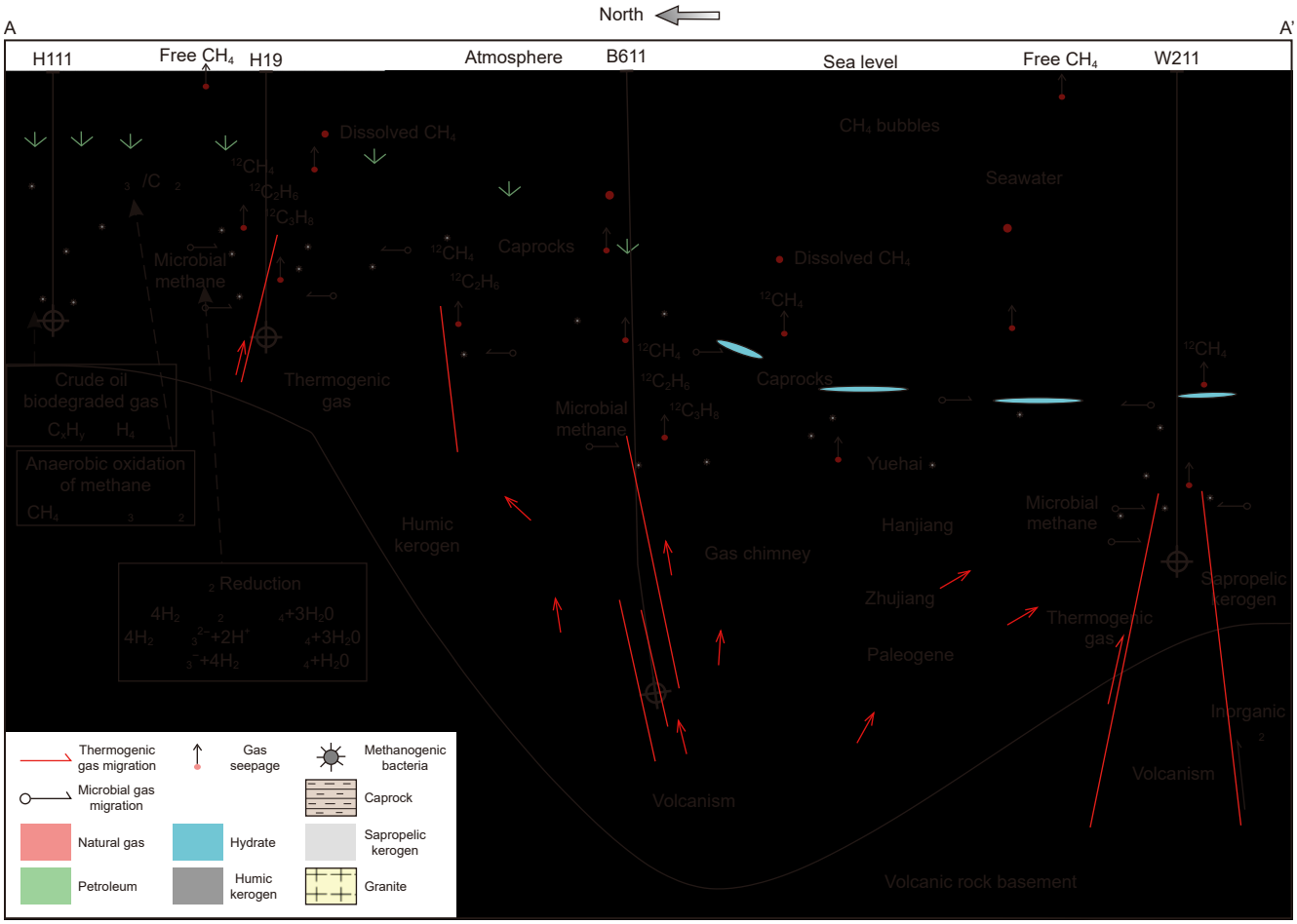

Fig. 13. Conceptual model of shallow gas accumulation in the Baiyun Sag-Panyu Uplift.

from −62.8‰ to −57.4‰ and hydrogen isotopes from −211‰ to −191‰ (Fig. 12(a)). Well 211 samples have δ^{13}C-CH_4 values around −50‰ and $C_1/(C_1–C_5)$ ratios exceeding 0.97, indicating a mix of biogenic and thermogenic gas. Distal Well W211, likely influenced by saline porewater, records δD-CH_4 values of −195‰ to −171‰ (Fig. 12(a)). The observed δD-CH_4–δ^{13}C-CH_4 reflects thermal maturation influences (Fig. 12(a)).

Carbon isotope fractionation coefficient ($\alpha c = [\delta^{13}C\text{-}CO_2 + 1000]/[\delta^{13}C\text{-}CH_4 + 1000]$) differs between methanogenic pathways. For CO_2 reduction, αc ranges from 1.049 to 1.095, while acetoclastic methanogenesis falls between 1.039 and 1.058 (Fig. 12(c)) (Whiticar, 1999). Acetate fermentation products show a δ^{13}C-CH_4–δ^{13}C-CO_2 anticorrelation, driven by preferential incorporation of ^{12}C into CH_4, enriching residual CO_2 in ^{13}C. Conversely, the carbon isotopes of hydrogenotrophic methane directly depend on the precursors, establishing a positive correlation (Rice and Claypool, 1981; Balabane et al., 1987). In the study area, mixed-source shallow gas reservoirs combine thermogenic gas (lower δ^{13}C-CO_2 values; higher δ^{13}C-CH_4 values) with biogenic gas, leading to a negative correlation between δ^{13}C-CH_4 and δ^{13}C-CO_2 (Fig. 12(c) and (d)). This overlap complicates genetic discrimination, causing CO_2-reduction-derived biogenic methane to be commonly misinterpreted as acetoclastic in origin.

5.3. Characterization of shallow gas accumulation

The studied shallow gas reservoirs exhibit distinct accumulation mechanisms despite comparable geochemical characteristics. Regional heterogeneity across the study area manifests in: (1) seawater depth gradients (180–2400 m), (2) reservoir stratigraphy (Yuehai–Hanjiang Formations north; Zhujiang–Zhuhai Formations south; Fig. 2), (3) thermogenic source facies (terrigenous Type II_2–III kerogen north vs. sapropelic organic matter south), (4) migration systems (fracture networks accessing paleo-reservoirs dominate the north; central mud diapirs and gas chimneys prevail; southern systems feature deep faults linked to CO_2-rich reservoirs), (5) thermal maturity (thermogenic maturity increases southward, progressing from mature-stage northern gases to higher-maturity central/southern accumulations). Reservoir depths cluster between 400 m and 1000 m below the sea floor. The exception is the B611 well in the subsidence center, as illustrated in Fig. 13.

Natural gas accumulation has stringent requirements for cap rock properties. Thick mudstones, commonly deposited in shallow marine environments, undergo weak diagenetic processes, allowing natural gas, especially compounds containing ^{12}C isotopes, to diffuse (Fig. 13). The accumulation of shallow gas is a dynamic accumulation process involving continuous loss and accumulation (Dang et al., 2008). In deep water areas, the escaping gas may migrate to shallow strata, forming natural gas hydrates with in-situ biogenic gas (Fig. 13). A notable example is the first trial production of natural gas hydrates conducted by the China Geological Survey in May 2017 in the Shenhu area of the Baiyun Sag. These hydrates exhibit δ^{13}C-CH_4 and δD-CH_4 values diagnostic of a CO_2-reduction methanogenesis (Dai et al., 2017). In shallow

water settings, the escaping methane-rich gas undergoes anaerobic oxidation with ions in seawater (Fig. 13). Substantial fluxes of methane may dissolve in seawater and subsequently escape into the atmosphere (Fig. 13), exacerbating greenhouse forcing. Given that shallow gas reservoirs are predominantly composed of thermogenic gas, favorable exploration areas typically correspond to regions with well-developed, high-quality reservoirs connected to deep source rocks via diapirs or fault conduits. Source rocks originate from the Zhuhai Formation or deeper strata, as the Zhujiang Formation and overlying units exhibit insufficient thermal maturity for large-scale natural gas generation. Although no commercial biogenic gas reservoirs have been discovered, their resource potential warrants further assessment given pervasive microbial activity indicators.

6. Conclusions

In the Pearl River Mouth Basin, South China Sea, shallow gas reservoirs within the Baiyun Sag and adjacent uplifts comprise mixed thermogenic and primary biogenic gas, with biogenic methane contributions $\lesssim$30%. Secondary biogenic gas from crude oil degradation is minimal, except in the northeastern structural belt. These reservoirs exhibit lower δ^{13}C-CH_4 (−52‰ to −34.4‰), elevated $C_1/(C_1–C_5)$ (>0.9), and enriched δ^{13}C ($C_2–C_3$) signatures relative to deeper counterparts, attributed to preferential escape of lighter components (^{12}C). $C_1/(C_1–C_5)$ (0.9−0.95) correlate positively with δ^{13}C-CH_4 below 0.95 but inversely at higher ratios. Non-hydrocarbon gases are typically present at low concentrations (N_2 <5%, CO_2 <1%), except in the W211 well, where CO_2 exceeds 60%, indicating localized CO_2 reservoirs in the southern Baiyun Sag.

Thermogenic gas primarily originates from type II_2-III kerogen cracking, supplemented by a sapropelic source in the southern sag. Microbial methane production, pervasive in mudstone and oil-sand extracts, proceeds dominantly by CO_2 reduction, resulting in δ^{13}C-depleted and δD-depleted CH_4, where porewater salinity gradients modulate δD-CH_4 variability (−211‰ to −171‰). The mixing of thermogenic gas induces an inverse δ^{13}C relationship between CH_4 and CO_2. Shallow-water gas reservoirs demonstrate distinct accumulation mechanisms compared to deep-water systems, differentiated by source facies, enrichment layers, migration pathways, natural gas maturity, and seawater depth gradients.

CRediT authorship contribution statement

Wei Si: Writing – original draft, Software, Writing – review & editing, Data curation, Conceptualization. **Du-Jie Hou:** Methodology, Funding acquisition, Conceptualization. **Xiong Cheng:** Writing – review & editing, Formal analysis, Methodology.

Declaration of competing interest

The authors declare that they have no known competing financial interests or personal relationships that could have appeared to influence the work reported in this paper.

Acknowledgments

We sincerely appreciate the editor's revision opportunity and the reviewers' constructive feedback. Their meticulous line-by-line scrutiny and insightful comments significantly enhanced this work's rigor and clarity. This work was supported by CNOOC (China) Ltd.'s productive scientific research project "Shallow gas enrichment mechanism and favorable exploration direction in the Baiyun Sag" (Grant No. 2022SKPS0082).

References

Balabane, M., Galimov, E., Hermann, M., Létolle, R., 1987. Hydrogen and carbon isotope fractionation during experimental production of bacterial methane. Org. Geochem. 11 (2), 115–119. https://doi.org/10.1016/0146-6380(87)90033-7.

Brassell, S.C., Wardroper, A.M., Thomson, I.D., Maxwell, J.R., Eglinton, G., 1981. Specific acyclic isoprenoids as biological markers of methanogenic bacteria in marine sediments. Nature 290 (5808), 693–696. https://doi.org/10.1038/290693a0.

Cheng, K.M., Jin, W.M., He, Z.H., 1987. Composition characteristics of light hydrocarbons in continental oil and condensate and their geological significance. Petrol. Explor. Dev. 14 (1), 34–43. https://doi.org/CNKI:SUN:SKYK.0.1987-01-004 (in Chinese).

Chung, H.M., Gormly, J.R., Squires, R.M., 1988. Origin of gaseous hydrocarbons in subsurface environments: Theoretical considerations of carbon isotope distribution. Chem. Geol. 71 (1–3), 97–103. https://doi.org/10.1016/0009-2541(88)90108-8.

Chung, H.M., Walters, C.C., Buck, S., Bingham, G., 1998. Mixed signals of the source and thermal maturity for petroleum, accumulations from light hydrocarbons: An example of the Beryl field. Org. Geochem. 29 (1–3), 381–396. https://doi.org/10.1016/s0146-6380(98)00063-1.

Clayton, J.L., Rice, D.D., Michael, G.E., 1991. Oil-generating coals of the San Juan Basin, New Mexico and Colorado, U.S.A. Org. Geochem. 17 (6), 735–742. https://doi.org/10.1016/0146-6380(91)90017-E.

Dai, J.X., 1993. Identification of coal formed gas and oil type gas by light hydrocarbons. Petrol. Explor. Dev. 20 (5), 26–32. https://doi.org/CNKI:SUN:SKYK.0.1993-05 (in Chinese).

Dai, J.X., Song, Y., Dai, C.S., Wang, D.R., 1996. Geochemistry and accumulation of carbon dioxide gases in China. AAPG Bull. 80 (10), 1615–1626. https://doi.org/10.1306/64eda0d2-1724-11d7-8645000102c1865d.

Dai, J.X., Ni, Y.Y., Huang, S.P., Peng, W.L., Han, W.X., Gong, D.Y., Wei, W., 2017. Genetic types of gas hydrates in China. Petrol. Explor. Dev. 44 (6), 887–898. https://doi.org/10.1016/s1876-3804(17)30101-5.

Dang, Y.Q., Zhao, W.Z., Su, A.G., Zhang, S.C., Li, M., Guan, Z.Q., Ma, D.D., Chen, X.F., Shuai, Y.H., Wang, H.T., Tan, Y.H., Xu, Z.Y., 2008. Biogenic gas systems in eastern Qaidam Basin. Mar. Petrol. Geol. 25 (4–5), 344–356. https://doi.org/10.1016/j.marpetgeo.2007.05.013.

Flores, R.M., Rice, C.A., Stricker, G.D., Warden, A., Ellis, M.S., 2008. Methanogenic pathways of coal-bed gas in the Powder River Basin, United States: The geologic factor. Int. J. Coal Geol. 76 (1–2), 52–75. https://doi.org/10.1016/j.coal.2008.02.005.

Gao, Y., Jin, Q., Zhu, G.Y., 2010. Genetic types and distribution of shallow-buried natural gases. Pet. Sci. 7 (3), 347–354. https://doi.org/10.1007/s12182-010-0076-y.

Hou, D.J., Cheng, X., Wei, L., Li, Y.J., Li, K.K., Zhang, Z.m., Zhang, H.y., Bian, J.j., Li, Y., Si, W., Jia, Z.j., He, J.h., Huang, Q., 2024. Oil and natural gas geochemistry in offshore China: Advances and challenges. Nat. Gas. Ind. B 11 (6), 631–644. https://doi.org/10.1016/j.ngib.2024.11.009.

Huang, B.J., Tian, H., Huang, H., Yang, J.H., Xiao, X.M., Li, L., 2015. Origin and accumulation of CO_2 and its natural displacement of oils in the continental margin basins, northern South China Sea. AAPG Bull. 99 (7), 1349–1369. https://doi.org/10.1306/02091514125.

Huang, G.H., Zhang, M., Hu, G.Y., Xiao, Z.Y., 2009. Geochemical study on oil-cracked gases and kerogen-cracked gases (II)-Discrimination methods between oil-cracked gases and kerogen-cracked gases. Sci. China Earth Sci. 52, 10–18. https://doi.org/10.1007/s11430-009-5020-x.

Huang, S.P., Li, J.Z., Wang, T.S., Jiang, Q.C., Jiang, H., Tao, X.W., Bai, B., Feng, Z.Q., 2022. Application of light hydrocarbons in natural gas geochemistry of gas fields in China. Annu. Rev. Earth Planet Sci. 50, 13–53. https://doi.org/10.1146/annurev-earth-070921-054917.

Hunt, J.M., 1996. Petroleum Geochemistry and Geology. W.H. Freeman and Company, New York, p. 743.

Jiang, Z.L., Du, H.L., Li, Y.J., Zhang, Y.F., Huang, Y.P., 2015. Simulation of gas generation from the Paleogene enping formation in the Baiyun Sag in the deepwater area of the Pearl River Mouth Basin, the South China Sea. Energy Fuel. 29 (2), 577–586. https://doi.org/10.1021/ef502284p.

Krzycki, J.A., Kenealy, W.R., Deniro, M.J., Zeikus, J.G., 1987. Stable carbon isotope fractionation by Methanosarcina barkeri during methanogenesis from acetate, methanol, or carbon dioxide-hydrogen. Appl. Environ. Microbiol. 53 (10), 2597–2599. https://doi.org/10.1002/bit.260300516.

Larter, S., di Primio, R., 2005. Effects of biodegradation on oil and gas field PVT properties and the origin of oil rimmed gas accumulations. Org. Geochem. 36 (2), 299–310. https://doi.org/10.1016/j.orggeochem.2004.07.015.

Li, J., Yan, Q.T., Zhang, Y., Liu, G.D., Wang, X.B., 2008. The special sealing mechanism of caprock for Quaternary biogenetic gas in Sanhu area, Qaidam Basin, China. Sci. China Earth Sci. 51, 45–52. https://doi.org/10.1007/s11430-008-5020-2.

Li, J., Li, Z.S., Wang, X.B., Wang, D.L., Xie, Z.Y., Li, J., Wang, Y.F., Han, Z.X., Ma, C.H., Wang, Z.H., Cui, H.Y., Wang, R., Hao, A.S., 2017. New indexes and charts for genesis identification of multiple natural gases. Petrol. Explor. Dev. 44 (4), 535–543. https://doi.org/10.1016/s1876-3804(17)30062-9.

Lin, Z.Y., Sun, X.M., Peckmann, J., Lu, Y., Xu, L., Strauss, H., Zhou, H.Y., Gong, J.L., Lu, H.F., Teichert, B.M.A., 2016. How sulfate-driven anaerobic oxidation of methane affects the sulfur isotopic composition of pyrite: A SIMS study from

the South China Sea. Chem. Geol. 440, 26–41. https://doi.org/10.1016/j.chemgeo.2016.07.007.
Liu, Q.Y., Jin, Z.J., Wang, X.F., Yi, J., Meng, Q.Q., Wu, X.Q., Gao, B., Nie, H.K., Zhu, D.Y., 2018. Distinguishing kerogen and oil cracked shale gas using H, C-isotopic fractionation of alkane gases. Mar. Petrol. Geol. 91, 350–362. https://doi.org/10.1016/j.marpetgeo.2018.01.006.
Liu, Q.Y., Wu, X.Q., Wang, X.F., Jin, Z.J., Zhu, D.Y., Meng, Q.Q., Huang, S.P., Liu, J.Y., Fu, Q., 2019. Carbon and hydrogen isotopes of methane, ethane, and propane: A review of genetic identification of natural gas. Earth Sci.